JOURNAL OF PROPULSION AND POWER
Vol. 17, No. 4, July–August 2001

Sensitivity of Mixed Subsonic–Supersonic Turbulent Mixing Layers

D. Chad Cottrell III* and Michael W. Plesniak†
Purdue University, West Lafayette, Indiana 47907-1003

Numerical predictions of compressible turbulent mixing layers have been performed for convective Mach numbers up to 0.7 ($M_C \leq 0.7$). This flow is particularly challenging to compute because the mixing layer consists of one supersonic stream and one subsonic stream, resulting in a mixed hyperbolic/elliptic solution. The FLUENT© computational fluid dynamics code, which incorporates a renormalization group k–ε turbulence model and the SIMPLEC solution algorithm, was used to perform the computations. Initially, predictions were performed for several different convective Mach numbers ($M_C = 0.2$, 0.5, and 0.7), and the computed results (mixing layer thickness, mean velocity, and turbulence parameters) were compared with experiments to benchmark the code. Following this qualification procedure, the sensitivity of the $M_C = 0.7$ case to disturbances was further investigated by introducing small perturbations to the boundary conditions and recomputing the mixing layer. Specifically, effects of perturbations to the secondary stream stagnation pressure and test section wall adjustment angle were investigated. It was found that the compressible mixing layer growth rate was significantly altered by small changes (<4%) in the secondary stream stagnation pressure. In addition, divergence or convergence of the test section walls of less than 3 deg resulted in appreciable changes in the streamwise pressure gradient and mixing layer development.

Nomenclature

A	=	test section cross-sectional area, m^2
a	=	speed of sound, m/s
b	=	10%ΔU mixing layer thickness ($y_{0.9\Delta U} - y_{0.1\Delta U}$), mm
C_b	=	empirical mixing layer growth rate constant
C_μ	=	parameter in k–ε turbulence model
db/dx	=	mixing layer growth rate
h	=	enthalpy, kJ/kgK
K	=	thermal conductivity, W/mK
k	=	turbulent kinetic energy, m^2/s^2
L	=	turbulent lengthscale (eddy scale), m
M_C	=	convective Mach number
P	=	pressure, kPa
R	=	ideal gas constant, kJ/kgK; or rate of strain term in Eq. (6), m^2/s^4
r	=	freestream velocity ratio, $\bar{u}_S/\bar{u}_P$
s	=	freestream density ratio, ρ_S / ρ_P
T	=	temperature, K
t	=	temporal coordinate, s
U_C	=	convective velocity, m/s
u	=	streamwise velocity component, m/s
$-\overline{u'v'}$	=	primary kinematic Reynolds shear stress (also $-\langle u'v' \rangle$), m^2/s^2
v	=	transverse velocity component, m/s
x	=	streamwise coordinate, mm
x_O	=	mixing layer virtual origin, mm
y	=	transverse coordinate, mm
α	=	wall adjustment angle, deg
γ	=	specific heat ratio
ΔU	=	freestream mean velocity difference, $\bar{u}_P - \bar{u}_S$, m/s
ε	=	turbulent dissipation rate, m^2/s^3
μ	=	dynamic viscosity, kg/ms
ν	=	kinematic viscosity, m^2/s
ρ	=	density, kg/m^3
τ	=	stress tensor
ω	=	relaxation parameter

Subscripts

eff	=	effective value (molecular plus turbulent contributions)
i	=	incompressible case
O	=	stagnation quantity
P	=	primary stream, Fig. 1, top
S	=	secondary stream, Fig. 1, bottom
T	=	turbulent contribution

Superscripts

$'$	=	turbulent fluctuating component
$\bar{}$	=	time-averaged value (also $\langle\,\rangle$)

Introduction

A NUMBER of recent studies have focused on gaining a better understanding of the fundamental flow physics of compressible turbulent mixing layers because they exhibit a reduced growth rate relative to their incompressible counterparts at the same velocity and density ratios. This reduction in growth rate is undesirable when rapid and efficient mixing of the two streams is required. Therefore, the goal of many of these studies has been to gain a better understanding of the mixing process and, ultimately, to develop practical methods of enhancing the compressible mixing layer growth rate. A practical application of supersonic mixing is the supersonic combustion ramjet (scramjet) engine, which has been proposed as a means of propelling hypersonic vehicles. One difficulty associated with the scramjet engine is that the turbulent mixing between the fuel and the oxidizer is inhibited, and, consequently, a longer combustor is required. Incomplete mixing of the fuel and oxidizer results in inefficient combustion and excessive pollutant formation. In addition to supersonic combustion, compressible mixing layers are also found at the thrust nozzles of some jet and rocket engines. For this application, mixing enhancement has been proposed as a means of reducing the noise generated by the exhaust of these engines. Noise abatement is becoming increasingly more important as stricter regulations are being introduced to limit the permissible noise level produced by aircraft.[1]

Received 10 August 2000; revision received 1 November 2000; accepted for publication 27 January 2001.

*Graduate Research Assistant, School of Mechanical Engineering. Member AIAA.

†Associate Professor, School of Mechanical Engineering, Maurice J. Zucrow Laboratories. Senior Member AIAA.

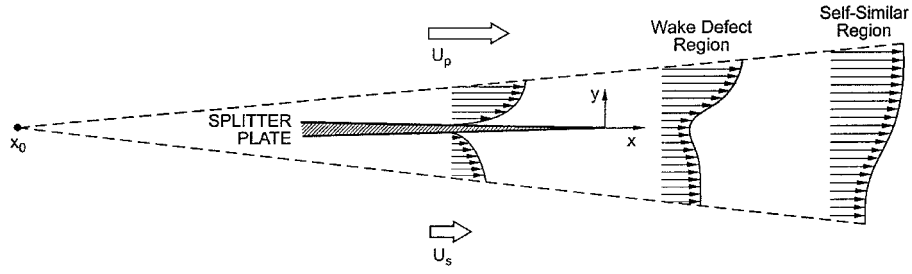

Fig. 1 Schematic of the two-stream planar mixing layer.

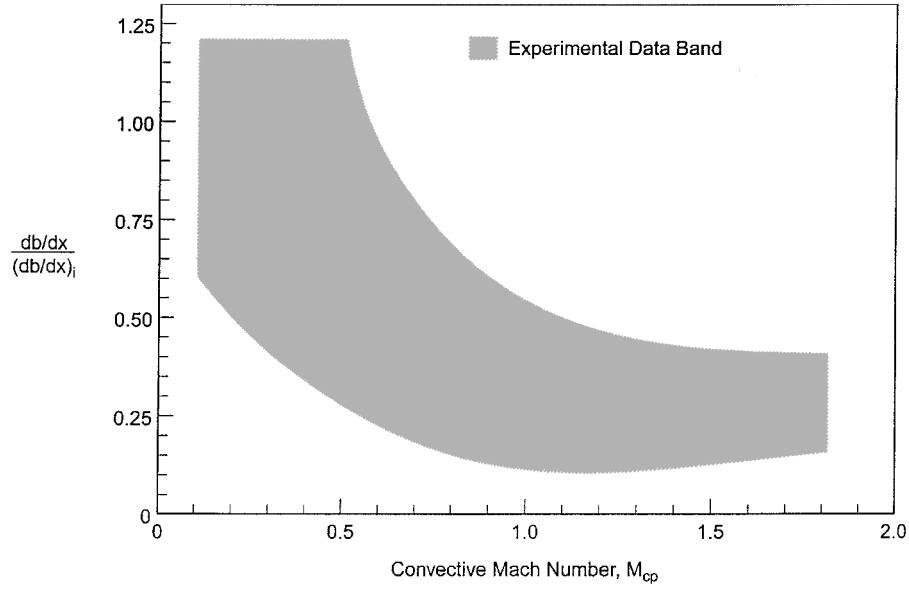

Fig. 2 Normalized mixing layer growth rates.

The two-stream planar mixing layer, shown schematically in Fig. 1, is a canonical flow that has been widely used to investigate the physics of mixing processes.[2–7] A mixing layer is formed when two streams of different velocities (and/or densities) merge downstream of the sharp trailing edge of a splitter plate. Throughout this manuscript, the high-speed stream will be referred to as the primary (shown on top), and the low-speed stream will be referred to as the secondary (shown on bottom), with properties denoted by P and S subscripts, respectively. Although several different definitions of the mixing layer thickness appear in the literature,[8] we define the mixing layer thickness b as the transverse distance between the locations where $\bar{u}_S + 0.1 \cdot (\bar{u}_P - \bar{u}_S)$ and $\bar{u}_S + 0.9 \cdot (\bar{u}_P - \bar{u}_S)$, that is, $10\%\Delta U$ thickness. The mixing layer growth rate is defined as db/dx. For the incompressible case, the self-similar growth rate (assuming that the entrainment velocity is proportional to the mean velocity difference) is expressed as

$$\left(\frac{db}{dx}\right)_i = C_b\left[\frac{(1-r)\left(1+s^{\frac{1}{2}}\right)}{\left(1+r\cdot s^{\frac{1}{2}}\right)}\right] \tag{1}$$

where $(r = \bar{u}_S / \bar{u}_P)$ is the freestream velocity ratio, $(s = \rho_S/\rho_P)$ is the freestream density ratio, and $C_b = 0.0825$ is an experimentally determined constant.[2] Experiments have shown that the growth rate of the incompressible mixing layer is governed by the formation and evolution of well-organized, large-scale two-dimensional spanwise structures, which convect downstream at a constant velocity.[9–11] Through the manipulation of these structures, it is possible to change the growth rate of incompressible mixing layers.[12–14]

Following the pioneering work of Brown and Roshko,[9] many investigations have shown that compressibility effects tend to inhibit the mixing process, thereby resulting in a reduced growth rate compared to an incompressible mixing layer operating at the same velocity and density ratios.[2–7] To quantify the level of compressibility, Bogdanoff[15] and Papamoschou and Roshko[7] assumed that organized large-scale structures were present in the compressible mixing layer. The convective velocity of these structures is $U_C = (a_S\bar{u}_P + a_P\bar{u}_S)/(a_P + a_S)$, whereas $(M_{CP} = (\bar{u}_P - U_C)/a_P$ and $M_{CS} = (U_C - \bar{u}_S)/a_S$ are the Mach numbers of the primary and secondary freestreams, respectively, relative to an observer moving at the convective velocity, U_C (Ref. 15). Therefore, M_{CP} and M_{CS} are usually referred to as convective Mach numbers, and they have been shown to provide a measure of the compressibility level of mixing layers. Note that, for the case of equal specific heat ratios $(\gamma_P = \gamma_S)$, the degree of compressibility is characterized by a single convective Mach number, defined as

$$M_C = (\bar{u}_P - \bar{u}_S)/(a_P + a_S) \tag{2}$$

Following Papamoschou and Roshko,[7] the effects of compressibility are illustrated in Fig. 2 on a plot of the normalized growth rates vs M_{CP}. The data band shown in Fig. 2 represents a compilation of experimental results from several different investigators.[6] To isolate the effects of compressibility, the growth rates have been normalized by the incompressible growth rates at the same velocity and density ratios using Eq. (1). The data all exhibit the same general trend: as M_{CP} increases, that is, as compressibility increases, the normalized growth rate decreases. At very high levels of compressibility $(M_{CP} > 1.0)$, the normalized growth rate appears to reach an average asymptotic value of about 0.3. Note that considerable scatter exists in the data for a variety of reasons, including different experimental facilities and techniques, different definitions of the mixing layer thickness, different initial conditions, etc.

Both numerical[16–18] and experimental[2–6] studies have suggested that the observed reduction in growth rate at higher compressibility

levels is associated with a change in the large-scale structure of the mixing layer. As M_{CP} increases, evidence of irregular three-dimensional structures has been found. These irregular structures cannot entrain as much fluid as the nearly round two-dimensional structures found in mixing layers originating from turbulent boundary layers on the splitter plate in the incompressible case. Several investigators[1,19,20] have attempted to enhance the compressible mixing layer growth rate, but their success has been limited, often resulting in only localized effects. One of the most promising methods appears to be the introduction of streamwise vorticity into the mixing layer.

The current work is concerned with the behavior of mixed, that is, subsonic–supersonic, mixing layers. Experimental and numerical investigations of canonical subsonic–supersonic mixing layers (i.e., zero pressure gradient and no shock or expansion waves) have proven rather challenging due to the hyperbolic behavior of the supersonic stream and the elliptic behavior of the subsonic stream, which make it difficult to match pressures at the splitter plate trailing edge. The objectives of this investigation are as follows. First, the performance of a commercial computational fluid dynamics (CFD) code was assessed for computations of mixed compressible two-stream planar mixing layers. To confirm the validity of the code, several different compressible mixing layers were computed, and the computational results were compared with the experimental data of Goebel and Dutton[2,3] and Goebel et al.[4] Second, the effects of perturbations to the boundary conditions were investigated to determine the sensitivity of compressible mixing layers to various parameters. Small changes to one of the boundary conditions (e.g., the secondary stagnation pressure, or the adjustment of the test section walls) were systematically introduced, and the mixing layer was recomputed. The results help to explain the reasons for the scatter in experimentally determined growth rates and also quantify the sensitivity of compressible mixing layers. The results provide design guidelines for investigators who wish to construct facilities in which to study clean, mixed compressible turbulent mixing layers. Possible methods of enhancing compressible mixing may also be inferred from results of this and similar future studies.

Code Description

The FLUENT© CFD code was selected for computing the dynamics of compressible two-stream planar mixing layers. FLUENT is a commercially available package that includes many options for modeling phenomena such as fluid flow, heat transfer, and chemical reactions. FLUENT solves a Reynolds-averaged form of the governing equations using a control volume-based finite difference method. The solution algorithm is based upon the SIMPLE (or, alternatively, SIMPLEC) algorithm (see Patankar[21]). An iterative line-by-line matrix solver is used, and multigrid acceleration is available to facilitate more rapid convergence. All variables are underrelaxed ($\omega < 1.0$) to maintain stability. Additional details of the FLUENT software may be found in the FLUENT reference manual.[22] Only the models and options used in the current study are discussed hereafter.

Governing Equations and Turbulence Model

In the current study, FLUENT was used to solve the Navier–Stokes equations in the following Reynolds-averaged form:

$$\frac{\partial \bar{\rho}}{\partial t} + \frac{\partial}{\partial x_i}(\bar{\rho}\bar{u}_i) = 0 \tag{3}$$

$$\frac{\partial}{\partial t}(\bar{\rho}\bar{u}_i) + \frac{\partial}{\partial x_j}(\bar{\rho}\bar{u}_i\bar{u}_j) = \frac{\partial \bar{\tau}_{ij}}{\partial x_j} - \frac{\partial \bar{P}}{\partial x_i} + \frac{\partial}{\partial x_j}(\overline{\bar{\rho}u_i'u_j'}) \tag{4}$$

$$\frac{\partial}{\partial t}(\bar{\rho}\bar{h}) + \frac{\partial}{\partial x_i}(\bar{\rho}\bar{u}_i\bar{h}) = \frac{\partial}{\partial x_i}\left(K\frac{\partial \bar{T}}{\partial x_i}\right) + \frac{\partial \bar{P}}{\partial t} + \bar{u}_i\frac{\partial \bar{P}}{\partial x_i} + \bar{\tau}_{ij}\frac{\partial \bar{u}_i}{\partial x_j} + \overline{\tau_{ij}'\frac{\partial u_i'}{\partial x_j}} - \frac{\partial}{\partial x_i}(\overline{\bar{\rho}u_i'h'}) \tag{5}$$

where the overbar represents a time-averaged quantity and the prime represents the fluctuating component from the Reynolds decomposition. In Eqs. (3–5), the density fluctuations have been neglected based on the assumption that $\rho' \ll \bar{\rho}$, that is, Morkovin's hypothesis.[23] Morkovin's hypothesis is a reasonable assumption for nonhypersonic, nonreacting flows without strong shock waves or significant heat transfer.[23]

FLUENT incorporates several different turbulence models. The standard k–ε turbulence model was used initially, but it failed to capture accurately the reduced growth rate of the compressible mixing layer.[8] Subsequently, a k–ε turbulence model based on renormalization group (RNG) theory was used to model the Reynolds stress tensor, turbulent diffusion of energy, and dissipation rate terms. Among other features, RNG theory provides an expression for the variation of effective viscosity ($\mu_{\text{eff}} = \mu + \mu_T$) with Reynolds number (or eddy scale).[22]

As in the standard k–ε model, transport equations for k and ε are solved. The transport equation for ε is

$$\frac{\partial \varepsilon}{\partial t} + \bar{u}_i\frac{\partial \varepsilon}{\partial x_i} = C_{1\varepsilon}\frac{\varepsilon}{k}\nu_T S^2 - C_{2\varepsilon}\frac{\varepsilon^2}{k} - R + \frac{\partial}{\partial x_i}\alpha\nu_T\frac{\partial \varepsilon}{\partial x_i} \tag{6}$$

where α is an inverse Prandtl number for turbulent transport, and $S^2 = 2S_{ij}S_{ij}$ is the modulus of the rate of strain tensor. Just like the effective viscosity, α is also allowed to vary with the Reynolds number (eddy scale) to improve the model's prediction in low Reynolds number flows; the constants $C_{1\varepsilon}$ and $C_{2\varepsilon}$ are also evaluated from RNG theory. In the high Reynolds number limit, the RNG model gives $\alpha = 1.39$, $C_{1\varepsilon} = 1.42$, and $C_{2\varepsilon} = 1.68$. The rate-of-strain term R in Eq. (6) is modeled using RNG theory.[22]

FLUENT's RNG k–ε model incorporates a compressibility modification to the standard transport equation for turbulent kinetic energy, k. The k-transport equation solved by FLUENT for compressible turbulent flow is

$$\frac{\partial}{\partial t}(\bar{\rho}k) + \frac{\partial}{\partial x_i}(\bar{\rho}\bar{u}_i k) = \frac{\partial}{\partial x_i}\left(\frac{\mu_T}{\sigma_k}\frac{\partial k}{\partial x_i}\right) + \bar{\tau}_{ij}\bar{S}_{ij} - \bar{\rho}\frac{C_\mu k^2}{\nu_c} \tag{7}$$

where

$$\nu_c = \nu + \nu_T \Big/ \left(1 + 2M_T^2\right) \tag{8}$$

and M_T is a turbulent Mach number defined by

$$M_T = \sqrt{k/\gamma RT} \tag{9}$$

Note that, in the high Reynolds number limit, the transport equation for k reduces to the compressibility modification proposed by Sarkar (see Ref. 24). Sarkar's modification has been shown to improve the predictions of compressible mixing layer growth rates (see Ref. 25).

Solution Procedures

The SIMPLEC solution algorithm was used for all computations because it eliminated convergence problems that were encountered initially when using the SIMPLE algorithm. For all variables except velocity, a power-law scheme (see Patankar[21]) was used to obtain values at the cell (control volume) faces. Velocity interpolation was accomplished via a viscosity weighted method, which is based on the continuity of shear stress for control volumes. This method results in more accurate prediction of turbulent kinetic energy inside shear layers, without excessive generation of turbulence.[22] Higher-order schemes (for example, QUICK) were investigated; however, they tended to create convergence problems and introduced oscillations into the solution, with no noticeable increase in accuracy. Multigrid acceleration was used to reduce the number of iterations required to reach convergence.

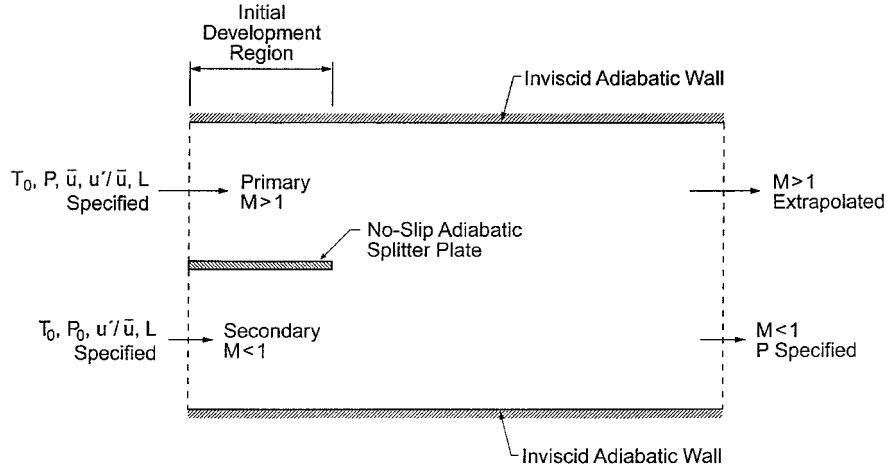

Fig. 3 Boundary conditions for the code validation study.

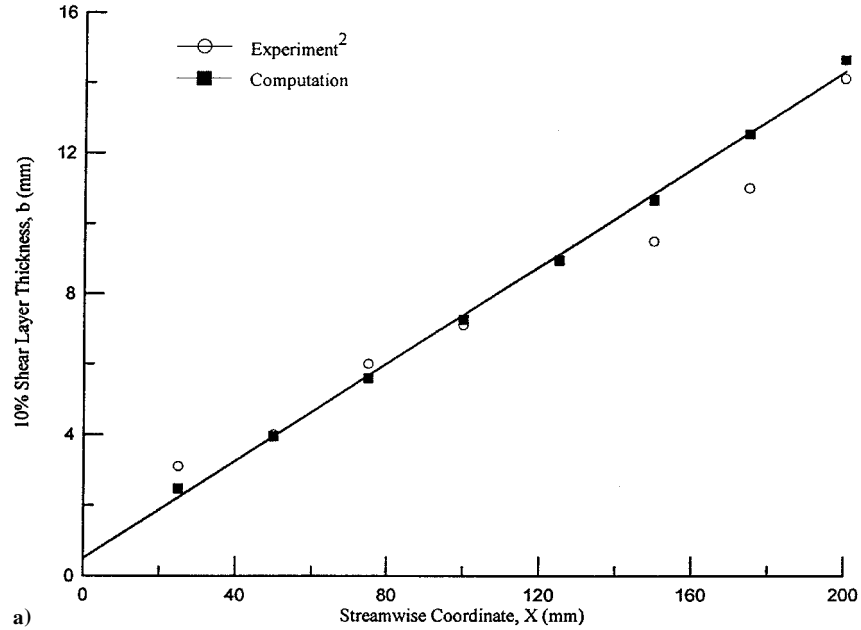

a)

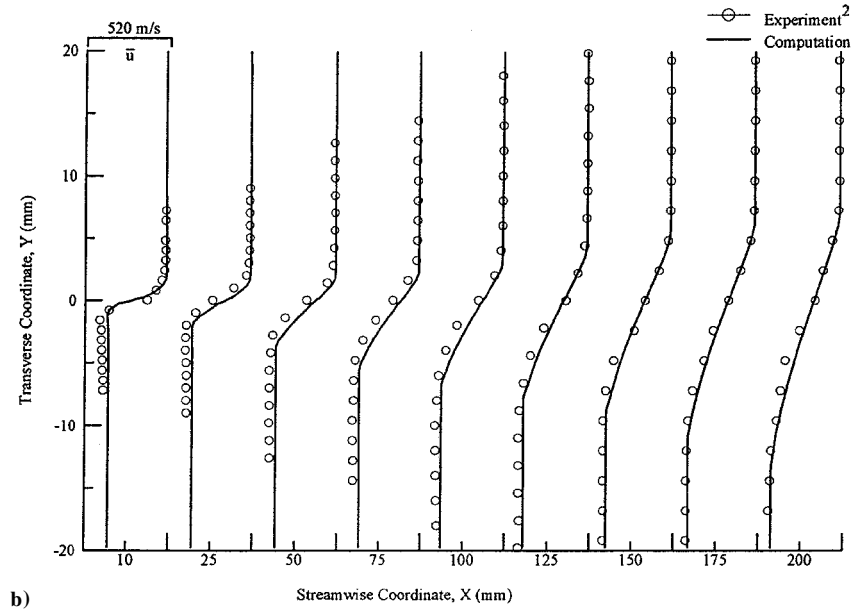

b)

Fig. 4 Computed and experimental a) growth rates and b) mean velocity profiles.

Results and Discussion

Code Validation

To evaluate the accuracy of the FLUENT CFD code, compressible mixing layers were simulated to duplicate the experimental conditions of Goebel and Dutton[2,3] and Goebel et al.,[4] and then the computed results were compared to experimental results. Using laser Doppler velocimetry (LDV), Goebel and Dutton measured mean and turbulence quantities in planar two-stream mixing layers operating at various levels of compressibility ($M_C = 0.2$, 0.5, 0.7, 0.9, and 1.0). FLUENT was not expected to successfully compute the highest M_C cases. (Note that FLUENT is primarily an incompressible code and that computations for $M_C > 0.7$ did not compare favorably with experiments: The $M_C = 0.9$ results were in poor agreement, and convergence could not be attained for the $M_C = 1.0$ case. This is attributable to shortcomings in the Reynolds-averaged framework, compressibility models, and SIMPLEC solution algorithm incorporated in FLUENT, as well as that the computation was two-dimensional whereas the flow becomes increasingly three dimensional with M_C.) Predictions of the $M_C \leq 0.7$ cases were performed to benchmark the predictions These were blind tests in the sense that no modeling constants were adjusted to force agreement with the experimental data. All results for $M_C \leq 0.7$ agreed well with experiments; hence, only the highest compressibility case ($M_C = 0.7$) will be discussed here.

The simulated experimental flowfield ($M_C = 0.7$) consisted of a supersonic (Mach 2.0) primary stream that merged with a subsonic (Mach 0.3) secondary stream downstream of a 0.5-mm-thick splitter plate. Both streams were air at a stagnation temperature of 285 K, and the splitter plate was tapered by 2.5 deg on the secondary side. At the splitter plate trailing edge, each stream was 23.75 mm high by 96 mm wide. Following their initial merger, the streams continued through the test section, which was approximately $47.5 \times 96 \times 500$ mm long. The test section walls were adjustable to minimize the streamwise pressure gradient. Experimental measurements were reported only for $0.0 < x < 225$ mm, due to the interaction of the mixing layer with the top or bottom wall boundary layers downstream of $x = 225$ mm. The $M_C = 0.7$ experimental

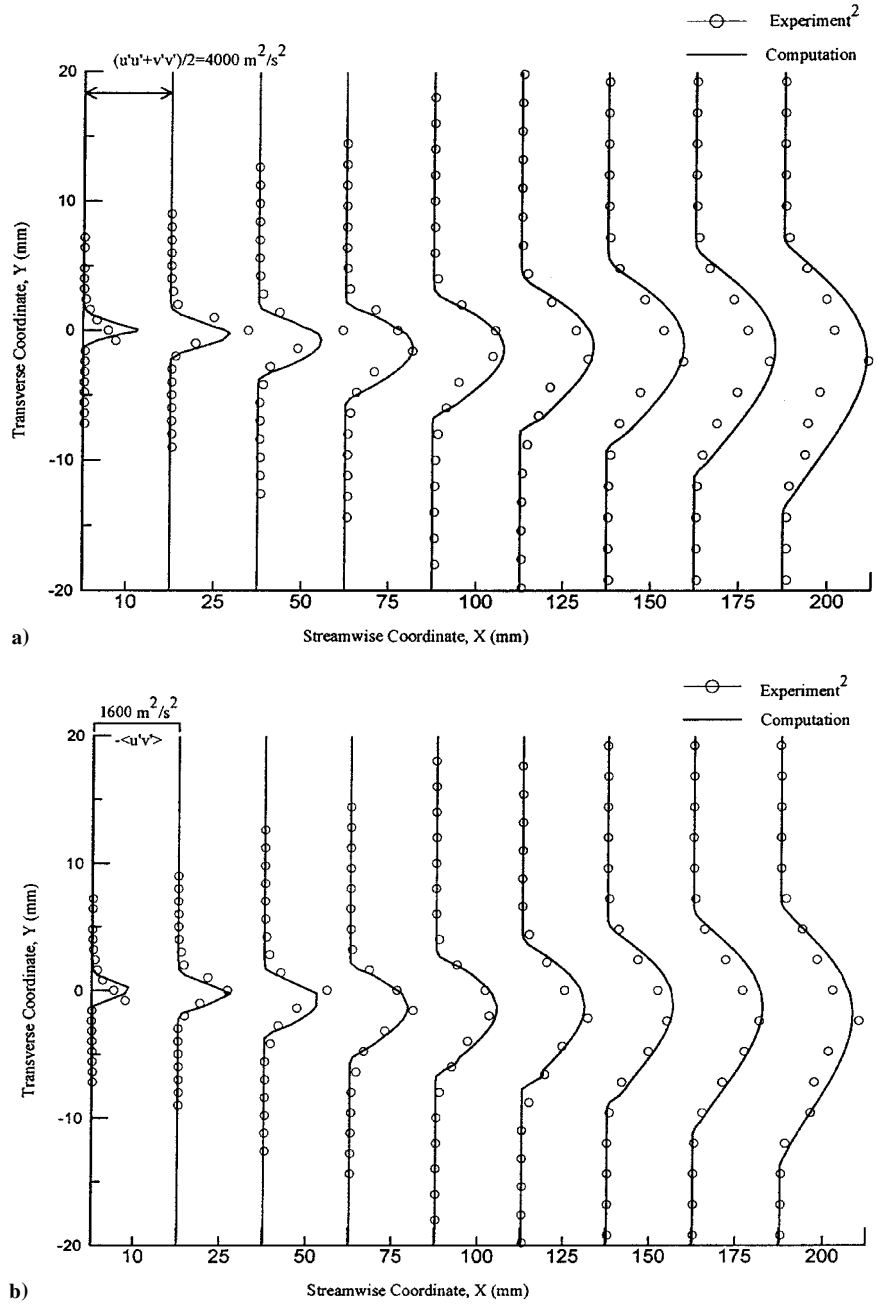

Fig. 5 Computed and experimental a) turbulent kinetic energy and b) primary Reynolds shear stress profiles.

operating conditions are listed in Table 1. Additional details of the experimental facilities may be found in Ref. 2.

The numerical predictions were two dimensional, which is appropriate only for the moderate M_C cases.[6,7] The geometry of the computed physical domain was chosen to match the experimental geometry as closely as possible, with a total height of 47.5 mm. The length was set to 300 mm, which includes a 75-mm-long initial development section, where the streams were separated by a 0.5-mm, adiabatic, no-slip splitter plate. The purpose of the initial development section was to allow boundary layers to grow on the splitter plate, to match the experimental conditions, before the two streams began to mix. Uniform inlet flow properties were specified for each stream. For the purpose of the initial code validation, the top and bottom walls were specified as adiabatic, parallel, and permitting slip. The specification of inviscid external walls and initial development region resulted in the best agreement with experiments, compared to other options considered.

Table 1 Experimental operating conditions (mean values) for $M_C = 0.7$ code validation

Quantity	Mean Value
M_C	0.7
M_P, M_S	1.96, 0.27
T_{PO}, T_{SO}, K	285, 285
u_P, u_S, m/s	499, 92
T_P, T_S, K	161, 281
a_P, a_S, m/s	255, 341
P (centerline static), kPa	53
ρ_P, ρ_S, kg/m^3	1.15, 0.66

All boundary conditions were specified to match the experiments as closely as possible. For the $M = 2.0$ primary stream, a supersonic inlet boundary condition was applied, that is, P, T_O, $\bar{u}$, $u'/\bar{u}$, and L were specified. For the $M = 0.3$ secondary stream, a subsonic (stagnation pressure) boundary condition was applied, that is, P_O, T_O, $u'/\bar{u}$, and L were specified. At the exit plane, the flow was partially subsonic and partially supersonic; therefore, a mixed boundary condition was applied. The mixed exit boundary condition consisted of a supersonic (extrapolated) exit boundary condition in the supersonic portion of the flow and a subsonic (static pressure specified) exit boundary condition in the subsonic portion of the flow. (For supersonic flows, a zeroth-order extrapolation from the upstream cells is applied for the exit boundary condition in the case where all of the fluid crossing the boundary is leaving the domain.) Several

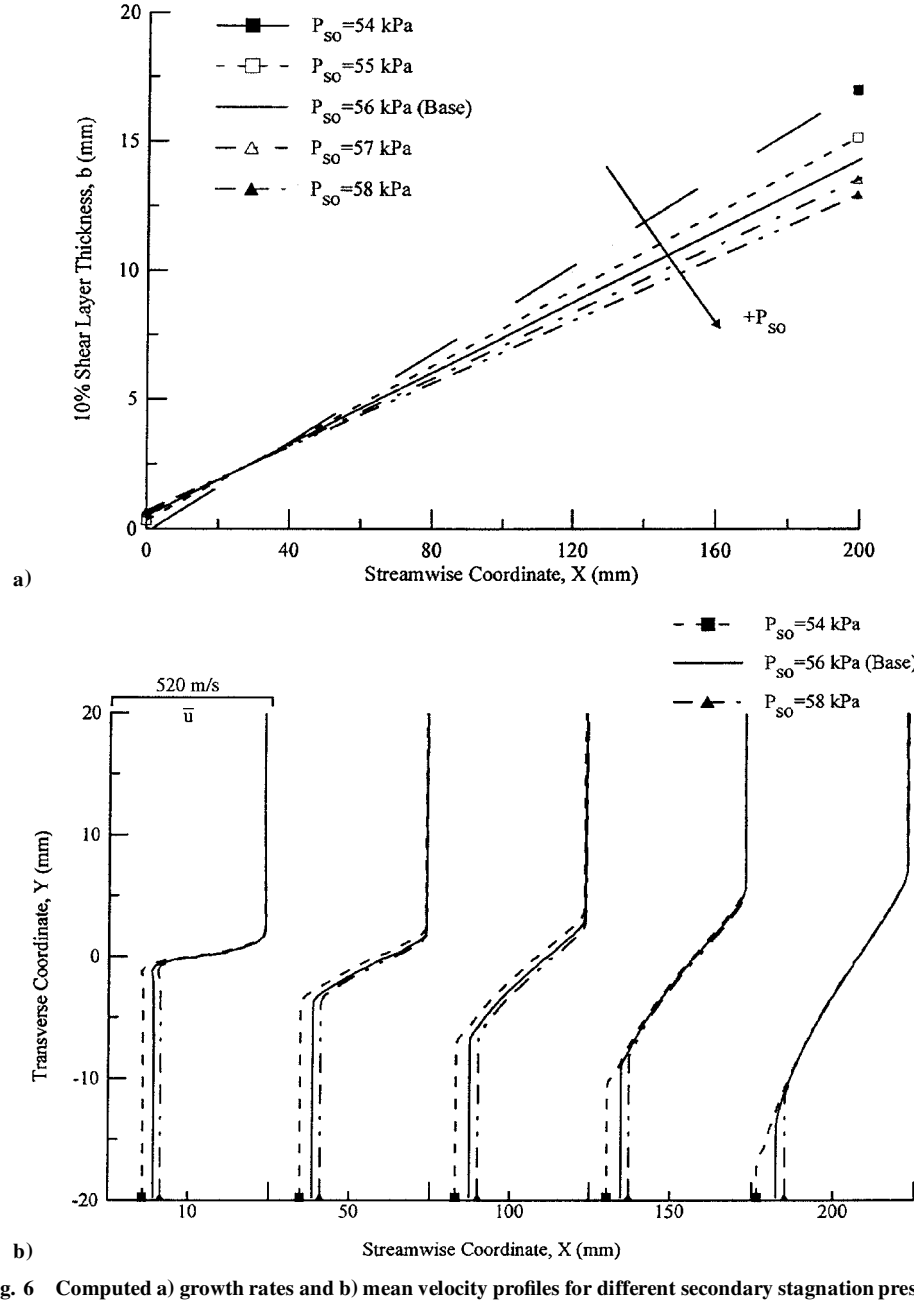

Fig. 6 Computed a) growth rates and b) mean velocity profiles for different secondary stagnation pressures.

iterations were performed to determine the transverse location that divided the supersonic and subsonic flow. A schematic of the physical domain and the applied boundary conditions is shown in Fig. 3. Several different grid sizes were investigated in a grid-independence study (100×50, 200×100, and 400×200). Grid independence was achieved using the 200×100 orthogonal grid. The grid points were clustered near the splitter plate trailing edge, where the gradients are expected to be largest. The solution was considered completely converged when the normalized residual (normalized by the residual at the second interation and summed over all cells) for each equation (except continuity) was on the order of $10^{-6} - 10^{-7}$. At this point, the residual for the continuity equation was typically on the order of $10^{-5} - 10^{-6}$. The FLUENT manual[22] suggests that a solution is typically converged when the normalized energy residual is on the order of 10^{-6} and all other residuals are below 10^{-3}. Therefore, the convergence criterion used in the current study is somewhat stricter than that suggested by FLUENT. All computations were performed on an IBM RS6000 model 380 workstation. For the 200×100 grid, nominal run times were on the order of 20 CPU hours, and the total memory core size was approximately 30 MB.

The computational and experimental results ($M_C = 0.7$) are compared in Figs. 4 and 5. Note that the lower compressibility cases ($M_C = 0.2$, 0.5) agreed at least as well as the $M_C = 0.7$ case.[8] Figure 4 shows the mean velocity profiles and mixing layer thickness (computed from the mean velocity profiles). Note that the computations capture the physics of the $M_C = 0.7$ mixing layer rather well, although the growth rate is overpredicted by approximately 15%. However, the experimental data points are somewhat scattered, whereas the computed mixing layer exhibits a linear growth, as expected in the self-similar region. Aside from slightly overpredicting the secondary stream mean velocity, the computed mean velocity profiles agree very well with the experiments. The computed turbulence quantities for $M_C = 0.7$ also agree well with experimental results (see Fig. 5), except in the wake region following the splitter plate trailing edge. This is not surprising because the flow in the wake region is very sensitive to the initial conditions. The computations predict the correct maximum values of turbulent kinetic energy and Reynolds shear stress but do not match the experimental profiles exactly, especially toward the end of the test section. Three-dimensional effects such as growth of boundary layers on the side walls of the test section become important in the downstream region. The primary kinematic Reynolds shear stress was computed from the following (two-dimensional) expression:

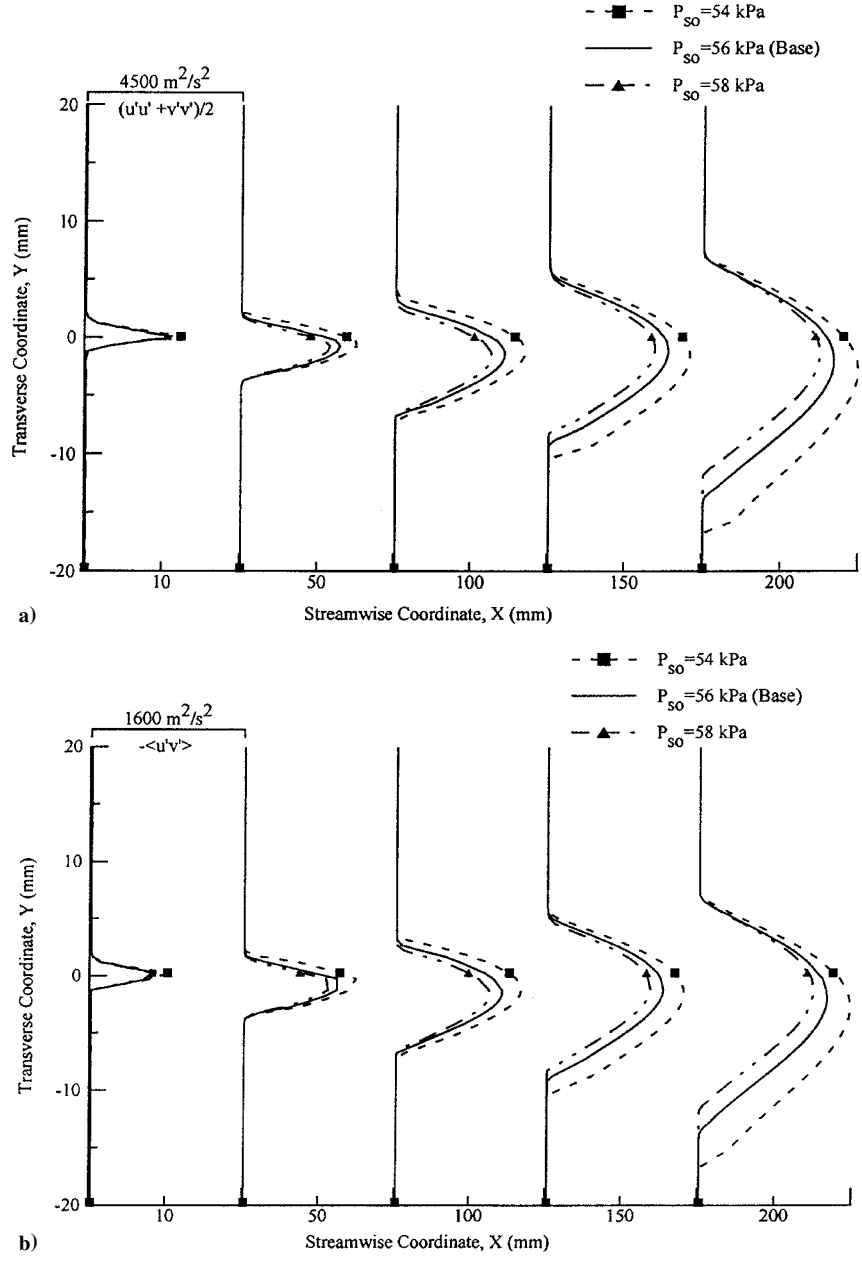

Fig. 7 Computed a) turbulent kinetic energy and b) primary Reynolds shear stress profiles for different secondary stagnation pressures.

$$-\langle u'v'\rangle \equiv -\overline{u'v'} = -C_\mu \frac{k^2}{\varepsilon}\left(\frac{\partial \bar{u}}{\partial y} + \frac{\partial \bar{v}}{\partial x}\right) \tag{10}$$

where $C_\mu = 0.0845$, that is, the limiting value for high Reynolds number turbulence. Note that the Reynolds shear stress [which involves approximations associated with differencing of the partial derivatives in Eq. (10)] agrees better with experiments than the turbulent kinetic energy (which is solved for directly from the governing equations). The discrepancy in the turbulent kinetic energy probably arises from the assumption of isotropic turbulence ($u' = v'$) implicit in the RNG k–ε model. Experimental results indicate that the streamwise turbulent fluctuations are considerably larger than the transverse fluctuations, especially at higher compressibility levels.[2,26]

In addition to the $M_C = 0.7$ benchmark case, other compressible mixing layers were simulated to qualify FLUENT. Results of all benchmark cases (omitted here for brevity) may be found in the thesis by Cottrell.[8] Based on the very good agreement with experiments, FLUENT was found to be acceptable for simulating compressible mixing layers for $M_C \leq 0.7$.

Perturbation Study

Further computations were performed at $M_C \approx 0.7$ to quantify the sensitivity of (and to identify possible mixing enhancement techniques for) the compressible mixing layer. The perturbation study was performed by introducing slight variations into the boundary conditions of the $M_C = 0.7$ code validation case. Similar sensitivity studies have already been performed for incompressible mixing layers.[14] For brevity, only select results are presented here; a complete discussion of the perturbation study is given by Cottrell.[8] Specifically, this paper presents perturbation results for two different variables: 1) the secondary stream stagnation pressure and 2) the angle of the external walls. The range of parameters studied was chosen based on typical experimental adjustments reported in the literature.[7,27] Table 2 summarizes the perturbations that were studied.

Table 2 Perturbations studied

Perturbation	P_{PO}, kPa	P_{SO}, kPa	α_P, deg	α_S, deg
Base case	391	56	0	0
P_{SO}	391	54	0	0
P_{SO}	391	55	0	0
P_{SO}	391	57	0	0
P_{SO}	391	58	0	0
Wall adjustment	391	56	0	2.5
Wall adjustment	391	56	2.5	0
Wall adjustment	391	56	2.5	2.5
Wall adjustment	391	56	0	−2.5
Wall adjustment	391	56	0	−1.25

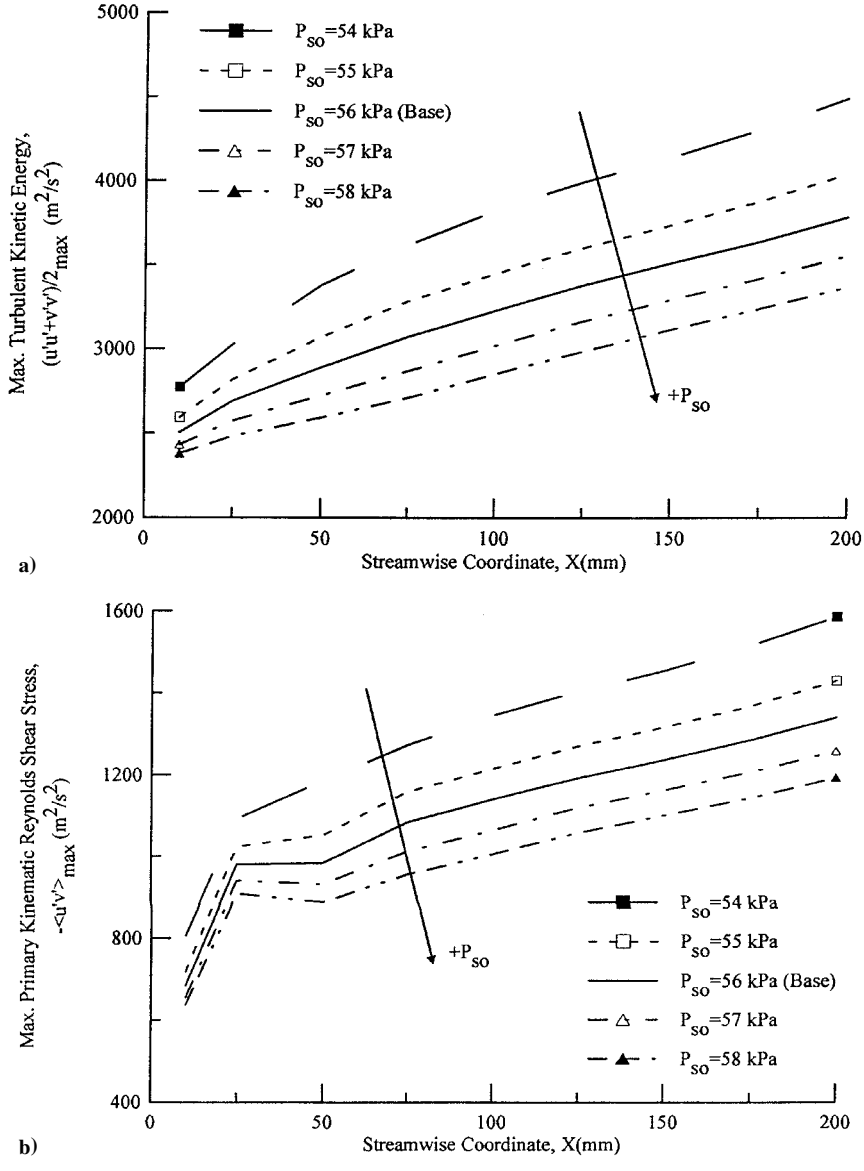

Fig. 8 Distributions of peak a) turbulent kinetic energy and b) primary Reynolds shear stress for different secondary stagnation pressures.

The procedure used to identify the effect of each perturbation is as follows. The perturbation was introduced; the flowfield was recomputed; and the perturbed results were compared with the original $M_C = 0.7$ code validation results (base case), which were already shown to agree with experiments. Thus, the original $M_C = 0.7$ code validation results serve as a reference case to identify the effects of perturbations on the mixing layer behavior. Note that, when investigating perturbations to the wall adjustment angle, no-slip walls were included in the base case, and the initial development region was omitted.

Secondary Stagnation Pressure

To quantify the sensitivity of the subsonic–supersonic mixing layer to small changes in the secondary stagnation pressure, computations were performed in which P_{SO} was perturbed ±1 kPa (±1.8%) and ± 2 kPa (± 3.6%), relative to the base case. Results of computations involving perturbations to the secondary stream stagnation pressure are presented in Figs. 6–8. In terms of absolute quantities, a decrease in P_{SO} (and secondary mass flowrate) resulted in an increase in the growth rate (Figs. 6 and 7). The increase in growth rate with decreasing P_{SO} is caused by insufficient secondary mass flow, which causes the mixing layer to spread further into the secondary stream to entrain the required amount of fluid. Figure 8 shows that the peak turbulence quantities (indicative of the amount of mixing) decrease with increasing secondary stagnation pressure. These trends are in agreement with the experimental results of Clemens,[6] who states that

> in a supersonic/subsonic mixing layer. . . [t]here is some subsonic Mach number for which the flow rate exactly meets the entrainment requirement. Additional flow will act to remove shear from the layer, thus reducing entrainment and only result in pressurizing the subsonic side, hence pushing the layer up and creating a strong shock at the splitter tip. Reduced flow increases the entrainment rate thus depressurizing the subsonic stream, resulting in an underexpanded supersonic stream.

Note that the peak values of the two-dimensional turbulent kinetic energy and primary Reynolds shear stress do not reach asymptotic values for downstream. This trend is exhibited in both the data and baseline computations. Thus, it must be concluded that the mixing layer has not achieved self similarity (of the turbulence quantities). This lack of similarity is due to the adverse pressure gradient in the test section.

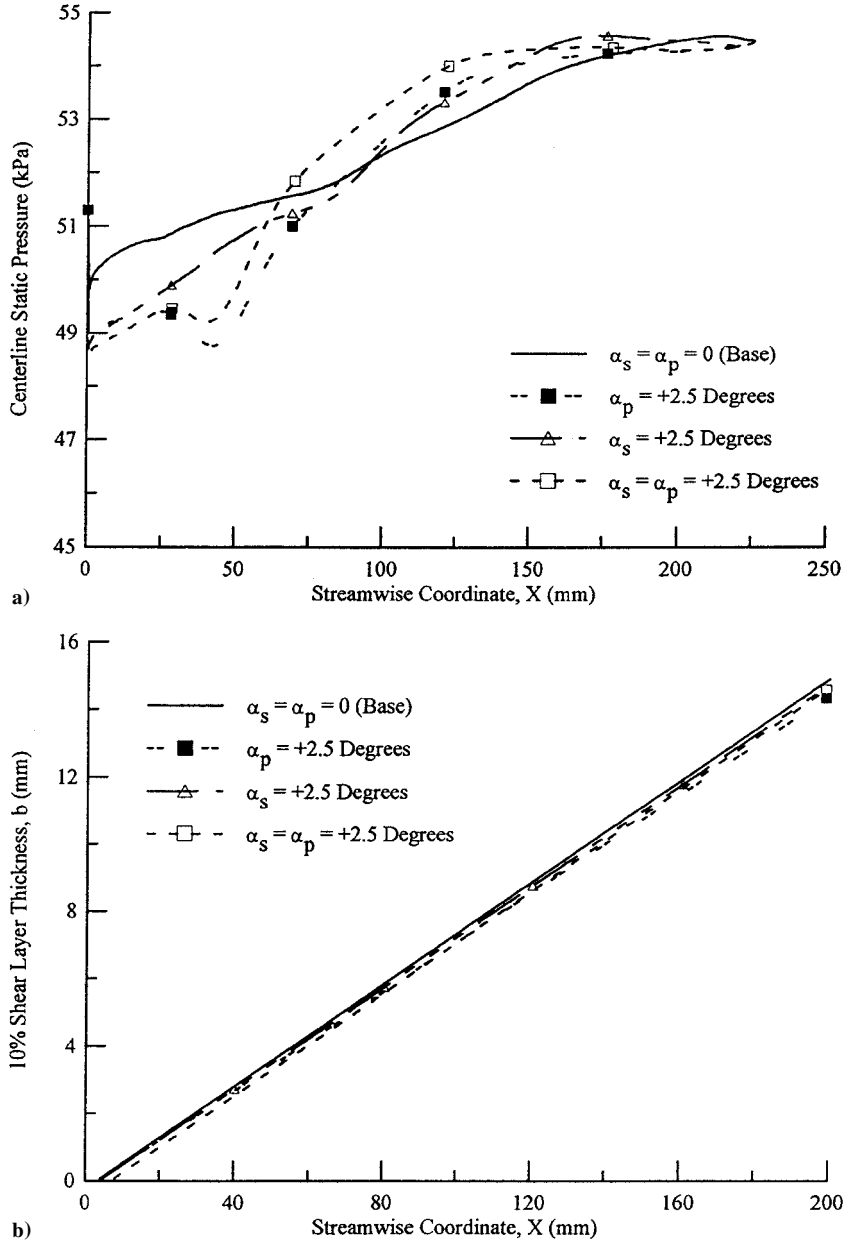

Fig. 9 Computed a) centerline static pressure distributions and b) mixing layer growth rates for different wall divergence angles.

Results of perturbations to the secondary stagnation pressure illustrate the precision necessary to study properly an undisturbed subsonic–supersonic mixing layer under the influence of zero pressure gradient. For example, these results indicate that a 1-kPa (1.8%) change in P_{SO} causes a 7% change in the growth rate and a 7% change in the peak value of turbulent kinetic energy. If the secondary stagnation pressure is not controlled precisely, the primary (supersonic) stream will pass through a compression or expansion wave at the entrance to the test section, and the mixing layer will deflect away from the horizontal. The results also suggest that, because it impacts the subsonic–supersonic mixing layer growth rate, manipulation of secondary stagnation pressure could lead to practical mixing enhancement techniques. This finding is extremely significant, for example, on the flow around the trailing edge of turbine vanes and blades.

External Wall Adjustment Angle

To identify the sensitivity of the subsonic–supersonic mixing layer to the wall adjustment angle, computations were performed in which the primary and/or secondary walls were adjusted ±1.25 or ±2.5 deg from the horizontal. Of primary concern was the influence of the wall adjustment angle on the streamwise pressure gradient and the resulting effect on the mixing layer dynamics. The literature[2,7] contains conflicting reports regarding the effectiveness of adjusting the walls to achieve a zero streamwise pressure gradient in mixed compressible mixing layers.

The wall adjustment angle α is defined as being positive if the walls are diverged away from the x axis. In other words, $\alpha > 0$ corresponds to a setting that causes an increase in flow area in the streamwise direction (divergence, $dA/dx > 0$), whereas $\alpha < 0$ corresponds to a setting that causes a decrease in flow area in the streamwise direction (convergence, $dA/dx < 0$). A wall setting parallel to the x axis corresponds to $\alpha = 0$, that is, the base case. The subscripts P and S refer to the primary and secondary (top and bottom) walls, respectively.

Divergence of Primary and Secondary Walls

Computations were performed to determine if diverging ($\alpha > 0$) the external walls would significantly affect the streamwise pressure

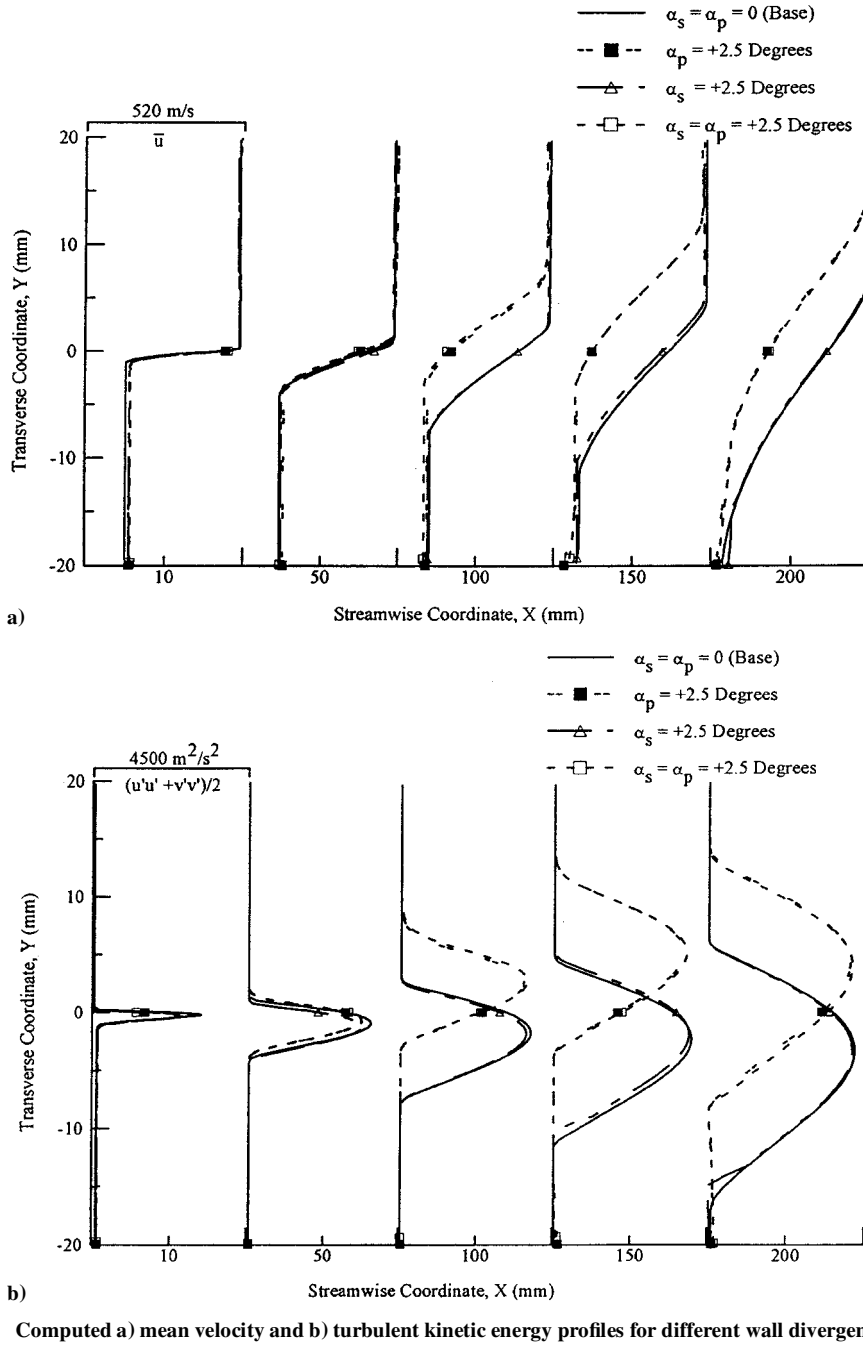

Fig. 10 Computed a) mean velocity and b) turbulent kinetic energy profiles for different wall divergence angles.

gradient or mixing layer behavior. The results are shown in Figs. 9–11. Note that the divergence angle for each wall was either 0 or +2.5 deg, which corresponds to a vertical displacement of about 10 mm (0.4 in.) at the exit plane of the physical domain ($x = 225$ mm). This displacement was based on the range of experimental adjustments reported by Papamoschou and Roshko[7] and Hall et al.[27]

The results illustrate that divergence of the primary wall has a greater effect on the mixing layer than divergence of the secondary wall. This is due to an expansion fan that emanates from the primary wall, where it begins to diverge (see Fig. 12). This expansion fan then impinges on the mixing layer and causes additional compression and expansion waves throughout the primary stream. Based on the first (Mach 2) characteristic emanating from the primary wall, the expansion fan begins to impinge on the mixing layer between $x = 40$ and 50 mm. The impingement of the expansion fan on the mixing layer results in a significant turning of the layer toward the primary stream. Note, in Fig. 10, that the mixing layer is deflected upward in the last three profiles ($x = 100, 150, 200$ mm), but not in the first two profiles ($x = 10, 50$ mm). This effect is absent in the first two profiles because the flow (near the mixing layer edge) has not yet been turned by the expansion fan at these locations. Similar turning of compressible mixing layers due to impingement of shock/expansion waves has also been observed experimentally.[2]

Although the expansion fan caused a noticeable deflection of the mixing layer, the growth rate was relatively unchanged (<4%, see Fig. 9b). Also, the profile shapes and peak values of the mean and turbulence quantities remained essentially unchanged. The most significant result of diverging the primary wall is that the mixing layer no longer remains straight. Instead, it develops bends because of the impingement of expansion and compression waves. This illustrates the importance of maintaining a perfectly straight primary wall if an undisturbed subsonic–supersonic mixing layer is to be studied. It also introduces the possibility of utilizing this effect to

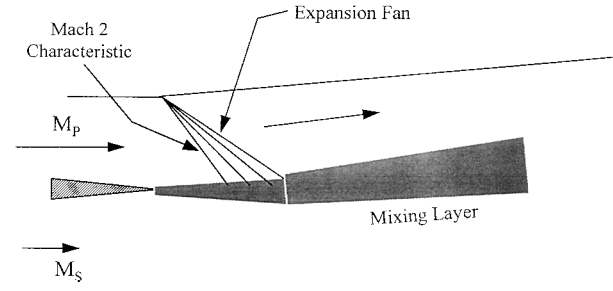

Fig. 12 Expansion fan resulting from primary wall divergence.

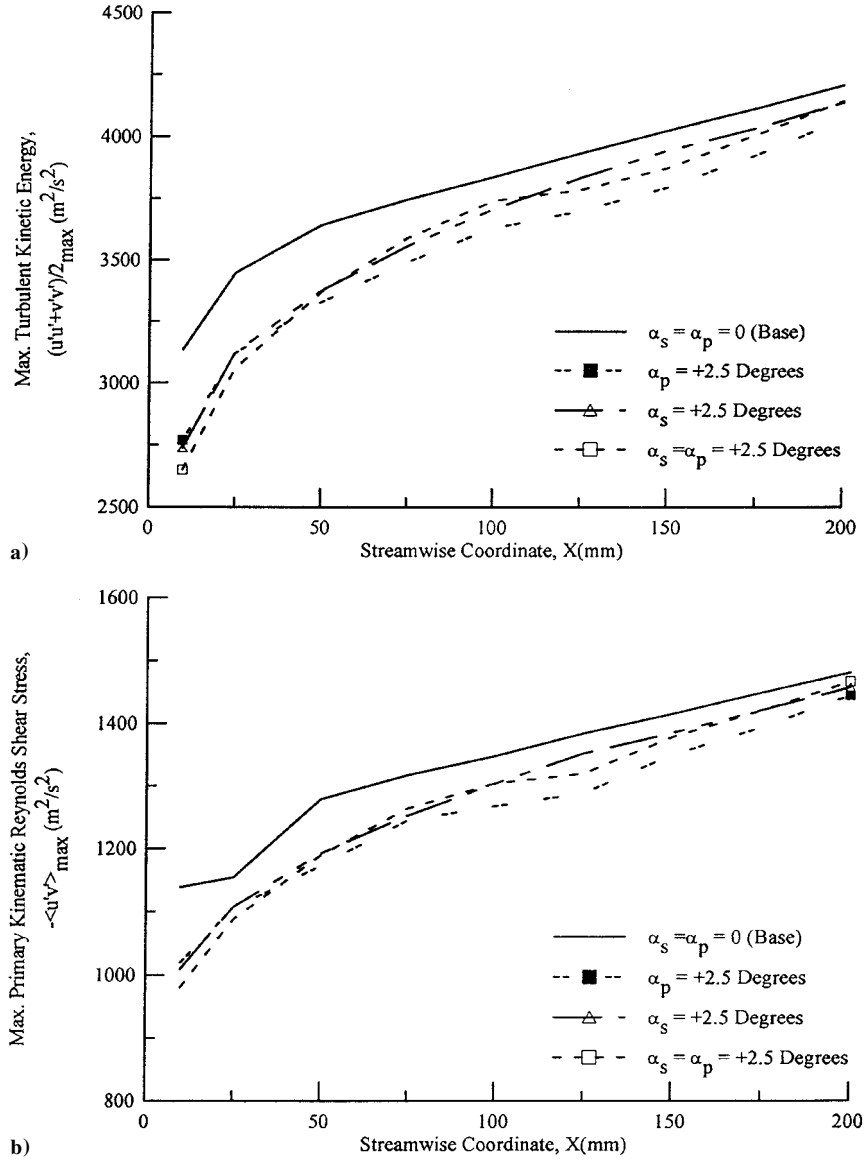

Fig. 11 Computed maximum a) turbulent kinetic energy and b) primary Reynolds shear stress distributions for different wall divergence angles.

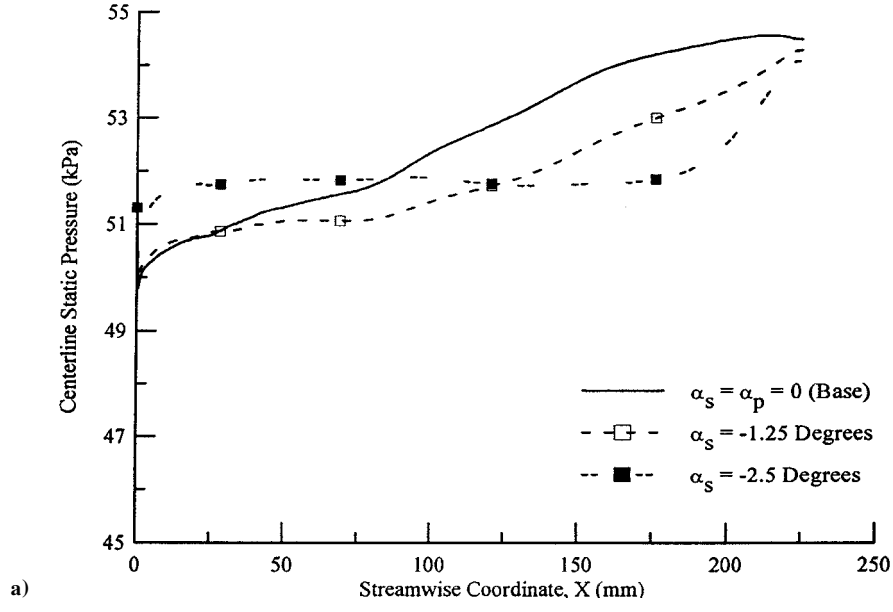

a)

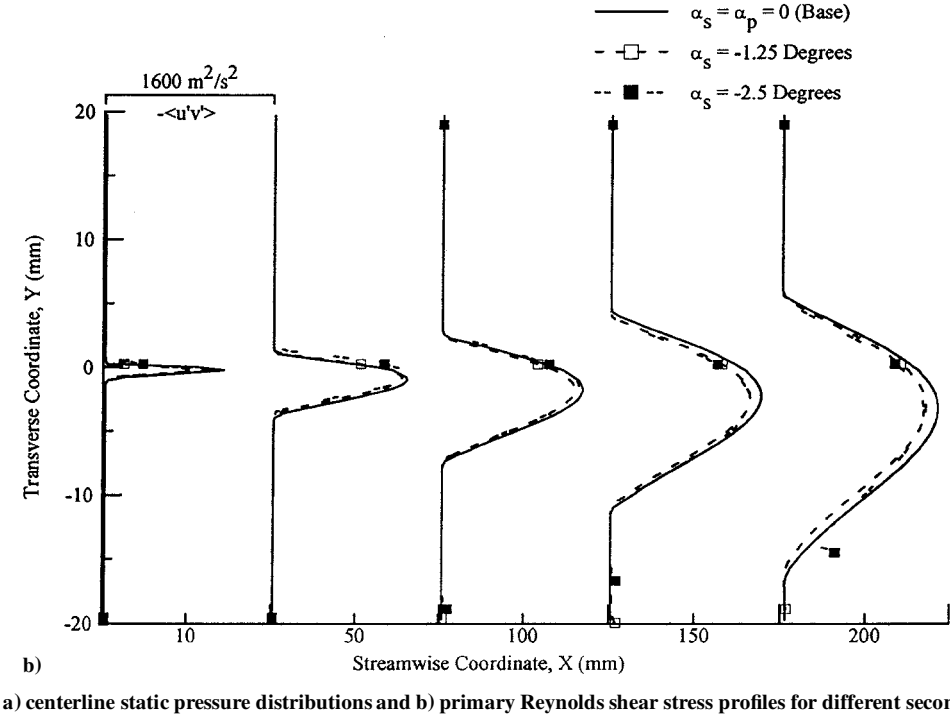

b)

Fig. 13 Computed a) centerline static pressure distributions and b) primary Reynolds shear stress profiles for different secondary wall convergence angles.

cause the mixing layer to oscillate up and down with time, possibly enhancing the transverse turbulent fluctuations and the growth rate. The numerical results of Liou et al.[28] suggested that, by causing the mixing layer to oscillate up and down with time, its growth rate may be increased significantly.

Convergence of Secondary Wall

Several subsonic–supersonic mixing layer experiments[6,27] have controlled the streamwise pressure gradient by slightly converging the secondary wall. Therefore, the effect of secondary wall convergence ($\alpha_S = -1.25$ or -2.5 deg) was also investigated, with $\alpha_P = 0$. Results are presented in Fig. 13.

Figure 13a shows that the shape of the centerline pressure distribution (and, hence, the local streamwise pressure gradient) is altered significantly by converging the secondary wall. Note that in both the experiments and computation that an adverse pressure gradient occurred in the test section. Recall that the exit plane static pressure (in the subsonic flow) was kept constant throughout all computations. The mean streamwise velocity profiles (not shown) remained relatively unchanged. The Reynolds shear stress decreased slightly due to the convergence of the secondary wall (see Fig. 13b), and the turbulent kinetic energy (not shown) exhibited a similar trend. Based on these results, adjustment of the secondary wall appears to be a practical means of controlling the streamwise pressure gradient in subsonic–supersonic mixing layers. In addition, manipulating the secondary wall angle does not introduce compression or expansion waves, which are undesirable when an undisturbed mixing layer is to be studied.

Conclusions

A numerical study of subsonic–supersonic planar mixing layers has been performed using the FLUENT CFD code, which is based on the SIMPLEC solution algorithm and incorporates an RNG k–ε turbulence model with compressibility correction. Based on the good

agreement of computed mean and turbulence quantities with experiments, this study has qualified FLUENT as a valid tool for accurately simulating mixing layers with $M_C \leq 0.7$. In addition, a perturbation study has quantified the sensitivity of subsonic–supersonic mixing layers to small changes in the imposed boundary conditions. Results regarding the influence of the external wall adjustment angle and the subsonic stream stagnation pressure on the mixing layer behavior and streamwise pressure gradient were discussed.

These results illustrate the precision with which the subsonic stream stagnation pressure must be controlled, for example, in an experiment, to study properly an undisturbed subsonic–supersonic mixing layer. It was found that changes of less than 4% in the subsonic stream stagnation pressure result in significant variations ($>10\%$) to the growth rate and peak turbulence quantities. The study also showed that small adjustments (≤ 2.5 deg) to the external wall angle cause appreciable changes in the local streamwise pressure gradient and mixing layer dynamics. Results of this and future studies may prove beneficial with respect to identifying practical mixing enhancement techniques for subsonic–supersonic mixing layers.

Acknowledgments

The authors wish to thank J. C. Dutton of the University of Illinois for providing the experimental data from Ref. 2 on disk, which enabled us to facilitate comparisons with our computations. We would also like to thank J. D. Hoffman and H. D. Thompson at Purdue University for many useful discussions during the course of this study.

References

[1]Gutmark, E. J., Schadow, K. C., and Ye, K. H., "Mixing Enhancement in Supersonic Free Shear Flows," *Annual Review of Fluid Mechanics*, Vol. 27, 1995, pp. 375–417.

[2]Goebel, S. G., and Dutton, J. C., "An Experimental Investigation of Compressible, Turbulent Mixing Layers," TR UILU ENG 90-4005, Dept. of Mechanical and Industrial Engineering, Univ. of Illinois at Urbana–Champaign, Urbana, IL, 1990.

[3]Goebel, S. G., and Dutton, J. C., "An Experimental Study of Compressible, Turbulent Mixing Layers," Dept. of Mechanical Industrial Engineering, TR UILU ENG 90-4005, *AIAA Journal*, Vol. 29, No. 4, 1991, pp. 538–546.

[4]Goebel, S. G., Dutton, J. C., Krier, H., and Renie, J. P., "Mean and Turbulent Velocity Measurements of Supersonic Mixing Layers," *Experiments in Fluids*, Vol. 8, No. 5, 1990, pp. 263–272.

[5]Elliott, G. S., Samimy, M., and Reeder, M. F., "Compressibility Effects on Large Structures in Free Shear Flows," *Physics of Fluids*, Vol. 4, No. 6, 1992, pp. 1251–1258.

[6]Clemens, N. T., "An Experimental Investigation of Scalar Mixing in Supersonic Turbulent Shear Layers," High Temperature Gasdynamics Lab., Rep. #T-274, Stanford Univ., Stanford, CA, 1991.

[7]Papamoschou, D., and Roshko, A., "The Compressible Turbulent Shear Layer: An Experimental Study," *Journal of Fluid Mechanics*, Vol. 197, 1988, pp. 453–477.

[8]Cottrell, D. C., "Investigation of Compressible Two-Stream Planar Mixing Layers," M.S. Thesis, Purdue Univ., West Lafayette, IN, School of Mechanical Engineering, Dec. 1996.

[9]Brown, G. L., and Roshko, A., "On Density Effects and Large Structures in Turbulent Mixing Layers," *Journal of Fluid Mechanics*, Vol. 64, 1974, pp. 775–816.

[10]Brown, G. L., and Dimotakis, P. E., "The Mixing Layer at High Reynolds Number: Large-Structure Dynamics and Entrainment," *Journal of Fluid Mechanics*, Vol. 78, 1976, pp. 535–560.

[11]Browand, F. K., and Winant, C. D., "Vortex Pairing: The Mechanism of Turbulent Mixing-Layer Growth at Moderate Reynolds Number," *Journal of Fluid Mechanics*, Vol. 63, 1974, pp. 237–255.

[12]Bell, J. H., and Mehta, R. D., "Development of a Two-Stream Mixing Layer from Tripped and Untripped Boundary Layers," *AIAA Journal*, Vol. 28, No. 12, 1990, pp. 2034–2042.

[13]Ho, C. M., and Huerre, P., "Perturbed Free Shear Layers," *Annual Review of Fluid Mechanics*, 1984, pp. 365–424.

[14]Dziomba, B., and Fiedler, H. E., "Effect of Initial Conditions on Two-Dimensional Free Shear Layers," *Journal of Fluid Mechanics*, Vol. 152, 1985, pp. 419–442.

[15]Bogdanoff, D. W., "Compressibility Effects in Turbulent Shear Layers," *AIAA Journal*, Vol. 21, No. 6, 1983, pp. 926, 927.

[16]Sandham, N. D., and Reynolds, W. C., "Compressible Mixing Layer: Linear Theory and Direct Simulation," *AIAA Journal*, Vol. 28, No. 4, 1990, pp. 618–624.

[17]Sandham, N. D., and Reynolds, W. C., "Three-Dimensional Simulations of Large Eddies in the Compressible Mixing Layer," *Journal of Fluid Mechanics*, Vol. 224, 1991, pp. 133–158.

[18]Leep, L. J., Dutton, J. C., and Burr, R. F., "Three-Dimensional Simulations of Compressible Mixing Layers: Visualizations and Statistical Analysis," *AIAA Journal*, Vol. 31, No. 11, 1993, pp. 2039–2046.

[19]Clemens, N. T., and Mungal, M. G., "Effects of Sidewall Disturbances on the Supersonic Mixing Layer," *Journal of Propulsion*, Vol. 8, No. 1, 1992, pp. 249–251.

[20]Shau, Y. R., and Dolling, D. S., "Exploratory Study of Turbulent Structure of a Compressible Shear Layer Using Fluctuating Pitot Pressure Measurements," *Experiments in Fluids*, Vol. 12, No. 4–5, 1992, pp. 293–306.

[21]Patankar, S. V., *Numerical Heat Transfer and Fluid Flow*, Hemisphere, Washington, DC, 1980, pp. 1–197.

[22]*FLUENT User's Guide*, Ver. 4.3, Fluent, Inc., Lebonon, New Hampshire, 1995.

[23]Morkovin, M. V., "Effects of Compressibility on Turbulent Flow," *The Mechanics of Turbulence*, edited by A. Favre, Gordon and Breach, New York, 1962, p. 367.

[24]Wilcox, D. C., *Turbulence Modeling for CFD*, 1st ed., DCW Industries, Inc., La Canada, CA, 1994, pp. 1–46.

[25]Choi, D., Sabnis, J. S., and Barber, T. J., "Application of an RNG k–ε Model to Compressible Turbulent Shear Layers," AIAA Paper 94-0188, Jan. 1994.

[26]Elliott, G. S., and Samimy, M., "Effects of Compressibility on the Characteristics of Free Shear Layers," *AIAA Journal*, Vol. 28, No. 3, 1990, pp. 439–445.

[27]Hall, J. L., Dimotakis, P. E., and Roseman, H., "Experiments in Nonreacting Compressible Shear Layers," *AIAA Journal*, Vol. 31, No. 12, 1993, pp. 2247–2254.

[28]Liou, T. M., Lien, W. Y., and Hwang, P. W., "Compressibility Effects and Mixing Enhancement in Turbulent Free Shear Flows," *AIAA Journal*, Vol. 33, No. 12, 1995, pp. 2332–2338.